Bull. Mater. Sci., Vol. 38, No. 7, December 2015, pp. 1851–1858. © Indian Academy of Sciences.

Synthesis and optical study of heat-treated ZnO nanopowder for optoelectronic applications

TAJ MUHAMMAD KHAN[1,2,*], TAYYABA BIBI[4] and BABAR HUSSAIN[1,3]

[1]National Institute of Lasers and Optronics (NILOP), Photonics Division, P.O. Nilore 45650, Islamabad, Pakistan
[2]Trinity College Dublin (TCD), School of Physics, Dublin, Ireland
[3]Department of Electrical and Computer Engineering, University of North Carolina at Charlotte, Charlotte, North Carolina, USA
[4]Department of Chemistry, University of Peshawar, Peshawar 45000, Pakistan

MS received 18 February 2015; accepted 2 April 2015

Abstract. **UV emitting ZnO nanopowder was chemically synthesized and subsequently subjected to heat treatment in oxygen atmosphere for potential optoelectronic properties. Characterization including Raman spectroscopy, photoluminescence, SEM, FT-IR and XRD were performed to see the effect of high temperature heat treatment and subsequently oxygen defects on the physical properties of ZnO powder. Chemically prepared product was highly pure polycrystalline w-ZnO with random crystallites orientation. Study showed a magnificent absorption of oxygen by the product as manifested by the decreased intensity of deep-level green emission and E_1 (LO) phonon mode. The phonon modes appeared at 276 and 970 cm^{-1} and which have been assigned to ZnO by the previous researchers under relaxed Raman selection rule were no longer found with heat treatment. UV emission was enhanced and the ratio of UV to green emission (I_{UV}/I_{green}) was correlated with the crystal structure and oxygen vacancies before and after heat treatment. FT-IR study established strong Zn-O bending and stretching bands at 356 and 498 cm^{-1}. SEM analysis demonstrated fine crystallites distribution in ZnO nanopowder with almost spherical morphologies. Reasonably, a more spherical and ordered morphologies with large grains were found with heat treatment. The investigated findings manifested improved structural and optical properties for various optoelectronic and biomedical applications of technological importance.**

Keywords. **Nanopowder; chemical synthesis; photoluminescence; Raman spectroscopy; semiconductor.**

1. Introduction

There is worldwide a strong drive to efficiently generate white light for many applications in lighting using ZnO and other semiconductor materials. Zinc oxide (ZnO) nanopowders are greatly used in the production of materials and components for different applications because of their specific attractive nano-structured properties.[1–3] As a direct wide bandgap material (3.37 eV at room temperature), ZnO is one of the most efficient emitter in the blue to ultraviolet (UV) spectral range and likely a candidate to replace materials like GaN in light-emitting laser diodes. Due to its strong UV emission stability and vacancies dependent green emission, ZnO is a potential material in optoelectronic for shorter-wavelength applications.[4] Particularly, ZnO nanopowders have drawn much attention during the last few years because of their novel optical and transport properties for newly emerging nanodevices.[5–8] Applications in optoelectronic, such as blue colour light-emitting phosphors, as nanorods UV light emitters, as fluorescence labels in medicine and biology, in controlling units as UV photodetectors and as high-flame detectors, as nanosensors of various gases, in cosmetic industry as a component of sun screens are significantly envisioned.[7–9] To prepare wurtzite-structured ZnO nanopowder, a number of synthesis techniques have been employed;[10–12] however, aqueous chemical route is rather simple, cost effective and conventionally easy compared to other cost rigorous methods.[9,12] Moreover, heat treatment is one of the processes employed to remove defects and improve structural, optical, electrical and magnetic properties.

In this research article synthesis of ZnO nanopowder is presented by a conventionally simple, relatively easy and economically cost-effective chemical route. Investigated findings include; luminescence, phonon modes, bonding characteristic and morphological properties before and after heat treatment at 1200°C. This temperature is quite appealing because newly observed phonon modes for the as-prepared sample were no longer found after heat treatment at 1200°C. Moreover, ratio of the UV-green emissions was correlated with crystal structure and oxygen vacancies. A comparison study was established for as-prepared and heat-treated samples in terms of crystalline structure, optical properties and perhaps most importantly in terms of UV emission has applications in biomedical and cosmetics. An analysis of the crystallite sizes determined by photoluminescence (PL) and X-ray diffraction (XRD) was made.

*Author for correspondence (tajakashne@gmail.com)

2. Experimental

2.1 *Preparation and heat treatment of ZnO nanopowders*

Zinc oxide nanopowders were prepared from Zinc nitrate $Zn(NO_3)_2{\cdot}4H_2O$ and NaOH chemical solutions. A quantity of 100 ml $Zn(NO_3)_2$ solution was taken and neutralized with 250 ml NaOH till the pH value of ∼12 was achieved, because the highly basic condition is conducive to the direct preparation of nanosize ZnO (equations 1–3). After neutralization, the conventional heating experiments were performed on magnetic stirrer. After completing the chemical reactions, the centrifuge process was employed to separate the solid and solution phases and the solids were washed free of salts with deionized (DI) water and ethanol. The white colour powder so obtained was calcinated at 90°C and then grinded for uniformity of the powder. The dry synthetic powders were weighed and the percentage yields were calculated from the expected total amount of ZnO based on the solution concentration and volume and the amount that was actually crystallized. Schematic diagram for the synthesis is illustrated in figure 1. The chemical equations for the synthesis of ZnO nanopowders are as below;

$$Zn(NO_3)_2 \rightarrow Zn^{+2} + 2NO_3^- \quad (1)$$

$$Zn^{+2} + 2OH^- \rightarrow Zn(OH)_2 \quad (2)$$

$$Zn(OH)_2 \rightarrow ZnO + H_2O. \quad (3)$$

A highly pure chemically prepared ZnO nanopowder was subjected to various heat-treatment temperatures in the range from 850 to 1200°C for different times (4, 6, 8, 10 and 12 h). Interestingly, the colour of the nanopowders mostly changed at 1200°C which reflects that mostly the heat-produced effects occur at this temperature and is quite appealing regarding experimental analysis. Crystalline zinc oxide is thermochromic, changing from white to yellow when heated and reverting to white on cooling in air. This colour change is caused by a small loss of oxygen to the environment at rather higher temperatures to form the non-stiochiometric $Zn_{1+x}O$, where at 800°C, $x = 0.00007$. The heat-treated sample at 1200°C was investigated along with the as-prepared sample. In literature, mostly ZnO-related research works have been reported at 1000°C;[13] however, we report here the effect of heat treatment on chemically prepared ZnO nanopowder at 1200°C and resulting in quite interesting consequences. The authors expect some interesting findings and properties at this temperature, because 1200°C is rather interesting regarding structural and optical properties. The interesting findings include the phonon modes at 276 and 970 cm^{-1} appeared for the as-prepared sample, which was no longer observed for the heat-treated sample.

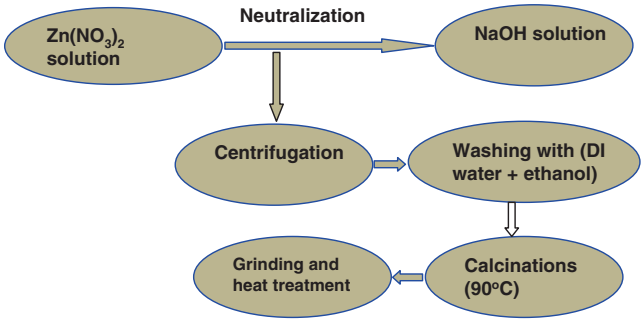

Figure 1. Schematic diagram for the chemical synthesis of ZnO nanopowder.

2.2 *Characterization techniques*

Chemically synthesized ZnO nanopowder was characterized for structural, morphological and optical properties. XRD analysis was carriedout with a Bruker D-8 Discover X-ray diffractometer equipped with a CuKα radiation ($\lambda = 1.54186$ Å). X-ray source was operated at 40 kV and 40 mA. The parallel incident X-ray beam was employed with a 0.12° roller slit at the secondary side. The measurements were performed by $\theta/2\theta$ scans in the 2θ angular range of 20–95°, with a step size of 0.02° and a scan rate of 2° min^{-1}.

In addition, instrumental broadening (B_I) caused by the slit width, sample size, sample penetration, imperfect focusing and non-monochromaticity of the beam (α_1 and α_2 for example) was carefully calibrated. Assuming Gaussian shape for the peaks, the broadening from the sample (B_s) was calculated through $B_{2s} = B_{2m} - B_{2I}$, where B_m is the measured broadening.

For investigating optical phonon modes and luminescence properties, a high-resolution Raman spectroscopy and PL system model MST-4000A was employed. The powder sample was focused in the image mode through an objective lens using illuminator. After focusing, the samples were subjected to He-Cd laser source emitting wavelengths of 442 and 325 nm for Raman and PL measurements, respectively. The signals were collected and detected in scan mode through the same objective lens and in an air cooled (−50°C) CCD detector. The laser lines 442 and 325 nm rejection was made by using the 442 and 325 nm cutoff filters. The Raman spectrum was taken in the range from 200 to 1200 cm^{-1}, while the PL spectra were taken from 200 to 900 nm using DM320 monochromator and ANDOR DV 401A-BV CCD software. Accumulative acquisition mode was used to reduce noise thermal fluctuation and to improve signal-to-noise ratio (S/N).

A Fourier transform infrared interferometer (PMQ II, Carl Zeiss) was used to measure the transmittance (T) and absorption (A) in the wavelength region of interest for optical applications (1000–4000 cm^{-1}).

Scanning electron microscopy (LEO 440i) attached with energy dispersive X-ray spectroscopy (EDS) was employed to study the surface morphology and elemental composition of the nanosized ZnO powder.

3. Results and discussion

3.1 *XRD analysis*

XRD analysis was used to identify exclusively crystalline structure, crystals orientation, phase purity and crystallites size of chemically prepared ZnO nanopowders. In figure 2, the sharp and intense diffraction peaks indicated that before and after heat treatment, ZnO nanopowders were highly polycrystalline and single phase with hexagonal (wurtzite) structure.[14] XRD spectra revealed that ZnO crystallites have preferred orientation along <101> direction. No additional diffraction peaks were observed related to impurity or any other phase of ZnO. It clearly indicated the synthesis of highly pure ZnO nanopowder by simple chemical aqueous route. The XRD results were also confirmed and supported by Raman and EDS studies, which have been mentioned henceforth. From figure 2 it was established that after heat treatment at 1200°C, the prepared ZnO nanopowder is polycrystalline and maintains wurtzite structure, which is thermally stable and hence shows no thermal transformation on heating. However after thermal treatment intensity of diffraction peaks was significantly higher than as-prepared sample. Heat treatment effectively removes defects and improves the crystalline structure. Peaks in the XRD spectra and their corresponding planes are as follows; $2\theta = 31.70°$ (100), $2\theta = 34.37°$ (002), $2\theta = 36.23°$ (101), $2\theta = 47.56°$ (102), $2\theta = 56.63°$ (110), $2\theta = 62.76°$ (103), $2\theta = 66.35°$ (200), $2\theta = 67.95°$ (112) and $2\theta = 69.02°$ (201). These noted peaks are closely matched and comparable to the mostly observed XRD peaks in similar studies for ZnO.[15–20] The two peaks in the XRD spectrum, (100) and (002) are labelled as *a*-axis and *c*-axis related peaks.[20,21] The presence of various other peaks corresponds to the planes other than (002) plane and illustrates polycrystalline nature of ZnO nanopowder.[22] This in-fact manifested synthesis of highly pure and good quality single-phase wurtzite ZnO nanopowder through a simple chemical method. For further information on crystallinity of chemically prepared ZnO nanopowder, crystallite size was incorporated. The average crystallite size (D) was determined using the Scherrer's formula:[23]

$$D = \frac{0.9\lambda}{\mathrm{FWHM}\cos\theta},$$

where D is the average crystallite size in nm, λ the X-ray wavelength in nm and θ is the Bragg's angle in radians.

The calculated average crystallite sizes before and after heat treatment at 1200°C, i.e., the regions of coherent scattering, were 23 and 25 nm, respectively. To account for the effect of heat treatment on defect density in ZnO, dislocation density (δ) was taken into account and calculated by using the grain size with the following formula:[24]

$$\delta = \frac{15}{aD}\left(\frac{\lambda}{D\cos\theta} - \beta\right)\frac{1}{\tan\theta},$$

where D, a, β and λ are the grain size of crystallites, lattice parameter, full-width half maximum and X-ray wavelength, respectively,

The value of dislocation density is quite high for the as-prepared sample (5.322×10^{15} m^{-2}) compared to heat-treated sample (1.1236×10^{14} m^{-2}).

The values of lattice parameters a and c for the nanosize ZnO were calculated using the following equation:[25]

$$\frac{1}{d^2} = \frac{4}{3}\left(\frac{h^2 + hk + k^2}{a^2}\right) + \frac{l^2}{c^2},$$

where h, k and l are the Miller indices, d the interplanar distance and a, c are the lattice parameters along x-axis and z-directions. The lattice constants for hexagonal ZnO nanoparticles reported in Joint Committee on Powder Diffraction Standards (JCPDS) match with the calculated one.

The interplanar parameter d was calculated by using the Bragg's formula:[26]

$$d = n\lambda/2\sin\theta,$$

where θ is the angle between normal of the diffracting plane and the incident X-ray, λ the wavelength of the X-ray and in our case was CuKα 1.5405 Å. The calculated values have been listed in table 1.

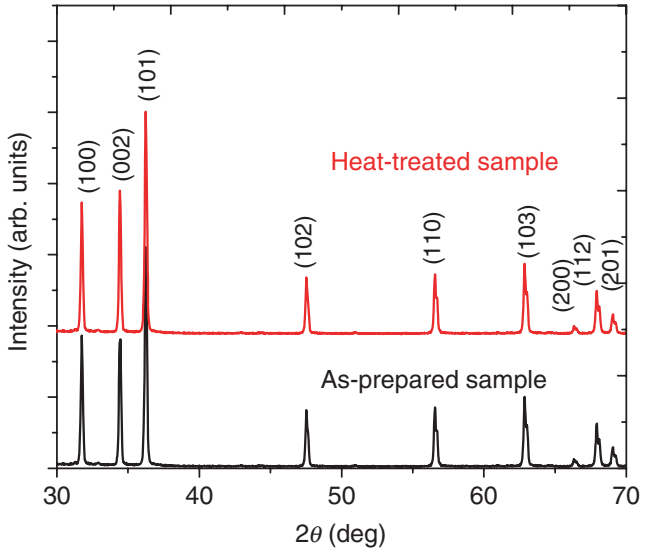

Figure 2. X-ray diffraction (XRD) pattern of as-prepared and heat-treated at 1200°C ZnO nanopowder (using CuKα radiation).

Table 1. Calculated values for some of the physical parameters for as-prepared and 1200°C heat-treated ZnO nanopowders.

Physical parameters	Heat-treated sample	As-prepared sample
Grain size (D)	25 nm	23 nm
Dislocation density (σ)	1.1236×10^{14} m^{-2}	5.322×10^{15} m^{-2}
Lattice parameter (c)	0.5231 nm	0.5167
Lattice parameter (a)	0.3252 nm	0.3218
Interplanar ($d_{(101)}$)	0.2605 nm	0.2594
Bandgaps	3.47 eV	3.47 eV

3.2 *PL study*

Because of its wide gap (3.37 eV at room temperature) and high exciton binding energy (60 meV), ZnO is a competing and attractive candidate as a luminescent material due to high radiative recombination efficiency for spontaneous emission even at room temperature and have found potential applications in cosmetic, biomedical and optoelectronics.

PL measurements were performed with He-Cd continuous laser source emitting excitation wavelength 325 nm. Figure 3 demonstrates room temperature PL spectrum of ZnO nanopowder before and after heat treatment. In general, ZnO shows four PL emissions; (a) a nearband edge (NBE) emission at 380 nm called UV emission, attributed to free-excitons recombination, (b) a blue emission at 460 nm because of intrinsic defects such as oxygen and zinc interstitials (c) a green emission (GL) at 540 nm, known as deep-level emission and is caused by impurities such as oxygen vacancies, zinc interstitials and (d) a red emission at 630 nm attributed to radiative recombination of a delocalized electron close to the conduction band with deeply trapped hole in the oxygen interstitials (Oi− centres) or may be due to oxygen and zinc anti-sites etc.[27–30] In our case the samples showed a prominent UV emission at 358 nm called near-band edge emission (NBE) and a deep-level green emission (DGE) at 525 nm; however after heat treatment intensity of the DGE decreased while that of the UV emission increased. This may be due to the effect of heat treatment on the intrinsic defects in the as-prepared ZnO nanopowders. The highest sharp\energy peak at 358 nm corresponds to the bandgap (3.47 eV) of ZnO and is assigned to the recombination of bound excitons.[31] The high bandgap value than that of the bulky ZnO (3.37 eV) can be attributed to the formation of nanosize ZnO powder. The GL has been studied extensively and various origins have been reported so far; however it can be explained here more explicitly as a single ionized oxygen vacancy results in a green emission because of the recombination of a photo-generated hole with a single ionized electron in the valence band.[32,33] The green emission may also result from the surface deep traps.[34,35] In particular, the origin of GL peak at around 2.3 eV is speculated to be an electron transition from the conduction band to Zn vacancy levels.[35] For the determination of particle size, UV peak wavelength was used in the equation based on effective mass approximation given by Brus.[28] The following equation derived using the effective mass model describe the particle size $D = 2r$ (r, radius) as a function of peak emission wavelength ($\lambda_p = 358$ nm) for the nanosized ZnO

$$r(\text{nm}) = \frac{-0.3049 + \sqrt{-26.23012 + 10240.72/\lambda_p(\text{nm})}}{-6.3829 + 2483.2/\lambda_p(\text{nm})}.$$

The particle size determined was 19.4 nm and closely matched with the XRD study. The comparison of crystallite size determined by XRD and PL support each other. Furthermore, the UV to green emission intensity ratio (I_{UV}/I_{green}) was considerably increased and obviously manifested to the improved crystalline structure of chemically synthesized nanosized pure ZnO.

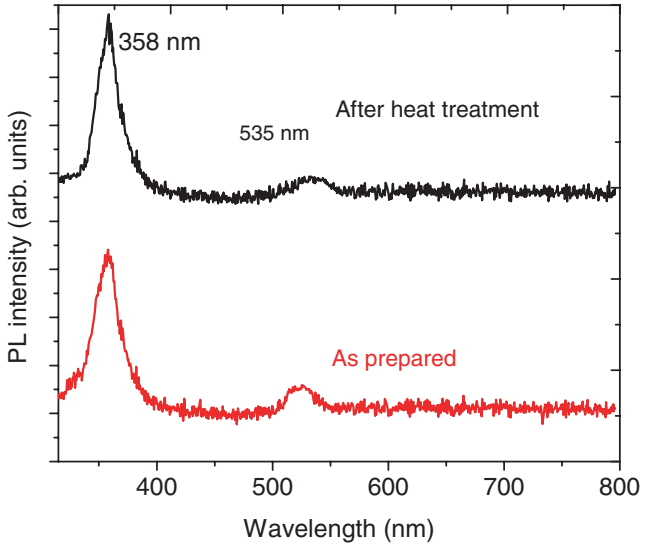

Figure 3. Room temperature PL spectra of as-prepared and heat-treated at 1200°C chemically synthesized ZnO nanopowder.

3.3 *Raman scattering analysis*

Raman scattering gives information about the crystal structure on the scale of a few lattice constants. The hexagonal (wurtzite) structure of ZnO belongs to the space group C_6v^4. Moreover at the point Γ of the Brillouin zone (BZ), the irreducible representation for optical phonon mode is given by the following equation;[36]

$$\Gamma_{opt} = A_1 + 2B_1 + E_1 + 2E_2.$$

In these modes, the E_2 modes are Raman active only while the other modes A_1, E_1 are both Raman and IR active. However, mode B_1 is both Raman and IR silent. Moreover, A_1 and E_1 are polar in nature, split into transverse (TO) and longitudinal (LO) components and all Raman active.[36,37] Both A_1 and E_1 are polar modes and split into transverse (TO) and longitudinal (LO) phonons with different frequencies due to macroscopic electric fields associated with the LO phonons. The different frequencies of A_1 and E_1 modes are due to short-range interatomic forces that cause anisotropy. As the electrostatic forces dominate the anisotropy in the short-range forces, the TO–LO splitting is larger than the A_1–E_1 splitting. For the lattice vibration A_1, atoms move parallel to the c-axis and for E_1 perpendicular to c-axis.

Figure 4 demonstrates the typical Raman spectrum of as-prepared and heat-treated ZnO nanopowder. The phonon bands observed at 328, 380, 435, 536, 571, 655 and 1145 cm^{-1} are the typical modes of ZnO.[38,39] The Raman shift at 435 cm^{-1} corresponds to the E_2 (high) principal phonon mode of ZnO. Mostly, the E_2 (high) mode, the so-called principal phonon mode, is the representative of band characteristic of ZnO wurtzite phase.[39,40] Interestingly,

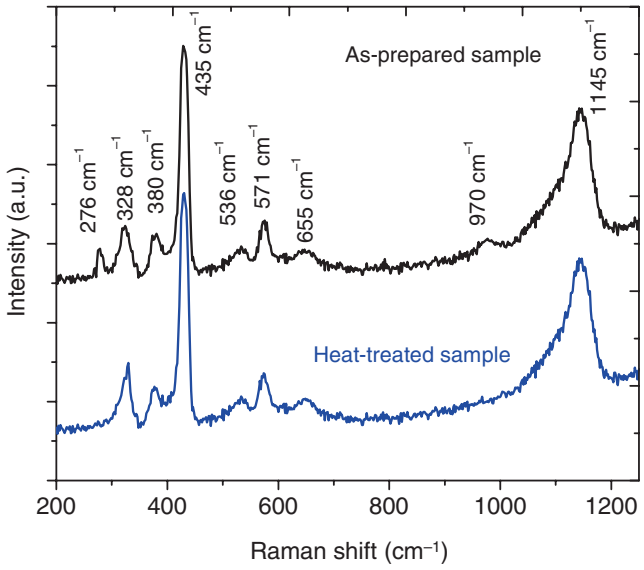

Figure 4. Room temperature Raman spectra of as-prepared and heat-treated at 1200°C chemically synthesized ZnO nanopowder.

let us dispute the fact that XRD does not evidence ZnO, the sharp peak in our Raman spectrum at 435 cm^{-1} is a clear manifestation of the E_2 (high) mode of wurtzite structure ZnO and its position is practically the same as for the bulk ZnO. Phonon dispersion relation that corresponds to the E_2 mode in ZnO at the Γ point does not show considerable dispersion. Therefore, even in ZnO nanopowder spectra, position of this mode is practically remaining unchanged.

Interestingly, the low- and high-frequency Raman peaks appeared at 276 and 970 cm^{-1} before heat treatment were no longer present after heat treatment (figure 4). These are not clearly understandable and further investigation is still required. However, an attempt has been made to explore their nature. The peak at 276 cm^{-1} may be due to oxygen vacancies, while the Raman band at 970 cm^{-1} can be associated with the B_1 (low) + B_1 (high) second-order scattering processes or it may be due to intrinsic defects (oxygen vacancies, Zn interstitials), which were removed after heat treatment and the peak is no longer practical. The two peaks that disappear after heat treatment may be due to the fact that heat treatment removed the existing defects that account for these observed peaks. The Raman shift at 380 cm^{-1} is the transverse phonon mode (A1 (TO)) of ZnO. The band at 655 cm^{-1} (2LO) is known to be the phonon mode of ZnO due to the second-order Raman processes ($E_2L + B_1H$), so called the multiple phonon scattering process.[41] The peaks at 536 and 571 cm^{-1} correspond to the longitudinal optical (LO) phonon modes of A_1 and E_1 modes. However, the mode at wavenumber 328 cm^{-1} encompasses the second-order Raman scattering from the E_2 (high)–E_2 (low) multiple scattering processes (2LO).[41,42] The newly found phonon peak at 1145 cm^{-1} was observed for both as-prepared and heat-treated samples with prominent behaviour. This band cannot be explained within the framework of single-phonon mode and attributed to multiple phonon scattering processes (2LO). The mode appears at 571 cm^{-1}, is the ZnO longitudinal optical (LO) phonon mode having E_1 symmetry and clearly shows the presence of defects (the defects attributed due to oxygen vacancies and Zn interstitials). The Raman analysis also supported purely wurtzite structure ZnO as we claimed in the XRD study. No additional peak corresponding to extrinsic defects and other phases were observed after heat treatment and reflected an idea that ZnO before and after heat treatment maintained its wurtzite structure. The Raman analysis provided an evidence that there is no phase transition according to the intensity changes of E_2 high mode, representative of the wurtzite structure ZnO. In addition to this, really a decrease in the intensity ratio of the E_1 (LO) peak to the E_2 (high) peak pointed out that heat treatment removed defects from the as-prepared ZnO nanopowders.[41,42] There was no drastic change in the Raman intensity, line shape and frequency shift in the observed phonon modes. No such changes have usually been attributed to the non-confinement of the optical phonons by the grain boundaries in ZnO materials.[43] These conclusions are in accordance with our XRD results described before.

3.4 *FT-IR analysis*

FT-IR measurement was demonstrated to understand molecular structure, chemical bonding and to identify elemental constituents of ZnO nanopowder. In this technique, almost all functional groups in a molecule characteristically absorb a definite range of frequency transmission of IR radiation and cause various molecule bonds to stretch and bend with respect to one another. Infrared transmission spectrum was taken in the range of our interest from 400 to 4000 cm^{-1}. Figure 5 shows FT-IR spectrum of chemically synthesized and heat-treated ZnO nanopowder. We observed two different bands as indicated, showing main absorption bands of ZnO nanopowder. Frequency bands of the spectrum located at 356 and 498 cm^{-1} could be assigned to bending and stretching vibrations of Zn–O (υ_{Zn-O}) bonds and well consisted with other reports.[44–46] These results are in good agreement with our XRD results and confirmed formation of purely wurtzite ZnO nanopowder. The result of IR spectrum of nanosize ZnO is generally influenced by particle size and morphology.[47] Our IR spectrum corresponds to ZnO nanoparticles with an average size of about 20 nm.[48] Moreover, before heat treatment, ZnO nanopowder sample shows a very feeble water absorption band of O–H molecules at 3300 cm^{-1} (not shown here).

3.5 *SEM analysis*

Surface morphology and atomic compositions of as-prepared and heat-treated ZnO nanopowders were investigated by scanning electron microscopy (LEO 440i) attached with EDS. Figure 6 shows SEM micrograph of as-prepared ZnO nanopowder taken with 5 Kx magnifications. This micrograph clearly demonstrated the formation of ZnO

nanopowder with almost spherical morphologies; however, bigger size particles were observed for the sample after heat treatment at 1200°C (figure 7) and in fact shows effect of thermal treatment on the morphology of nanosize materials.

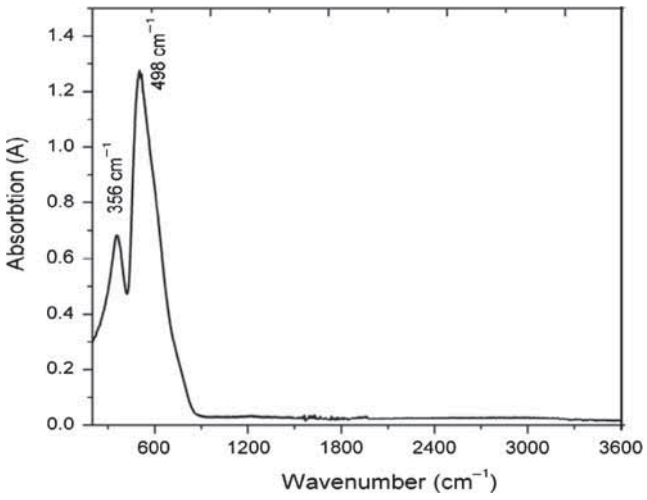

Figure 5. FT-IR spectra of chemically synthesized ZnO powder heat treated at 1200°C.

Moreover, particles distribution is narrow and fine, which reflects fine distribution of crystallites in ZnO nanopowders. The corresponding compositions were estimated from EDS (figure 8), which confirmed the formation of highly pure ZnO nanopowder with oxygen and zinc as the only elemental constituents. The prominent peak is the substrate-related peak. Our SEM analysis supports our results of XRD, PL, FT-IR and Raman spectroscopy. Moreover, ZnO crystallites were not distinguished in the samples at massive scale, as they were almost of the same sizes and shapes. All the zinc oxide crystallites in ZnO nanopowder upon heating at 1200°C showed similar morphologies with mixed smaller and bigger crystallites and a tendency to aggregation due to heat treatment[49] as evident from figure 7. Prior to heat treatment, initially the sample is composed of primary spherical particles with different agglomeration, orientation and arrangement and they become in ordered after heat treatment at 1200°C. The new particles (secondary particles) in the sample sintered at still higher temperatures give nanopowders with poorly defined morphology.[49] These obtained results allow one to propose a schematic representation for different steps followed by synthesis of nanopowders with particular emphasis on the agglomeration state of materials particles.

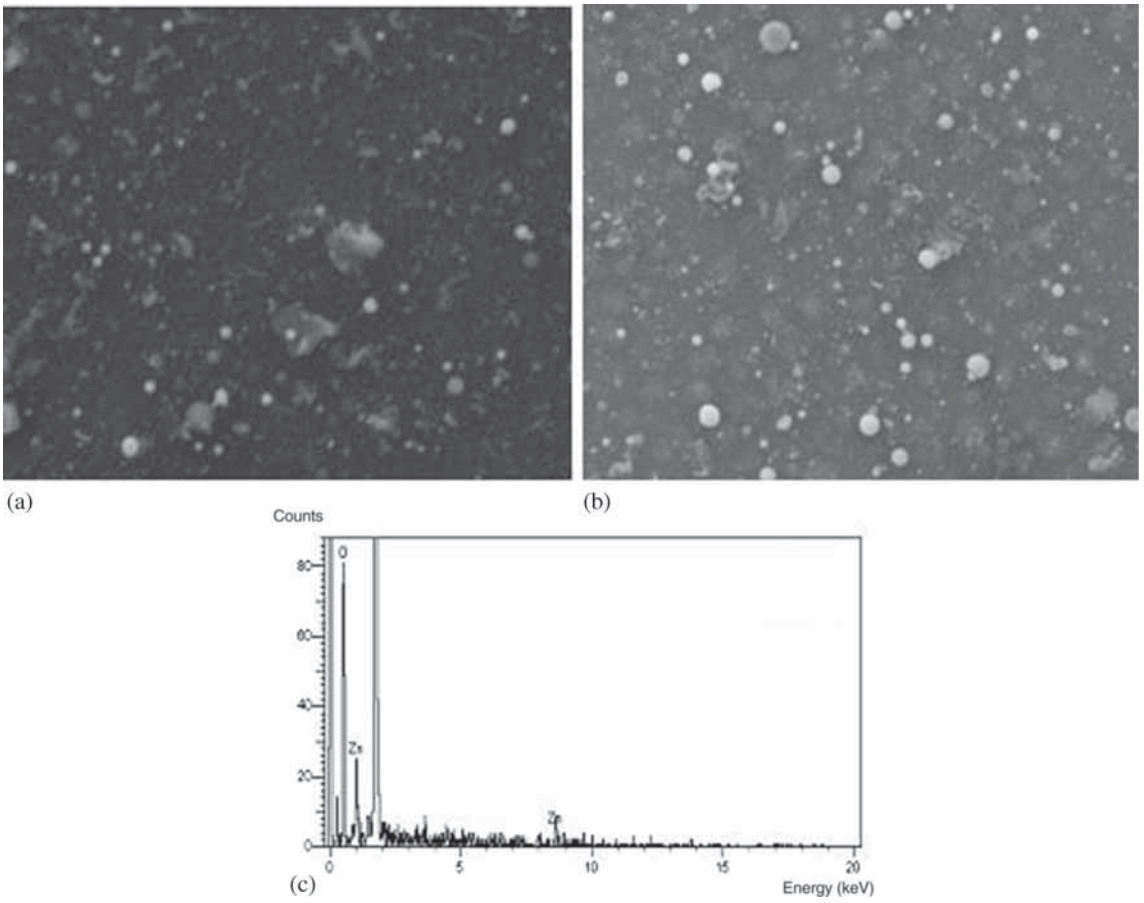

Figure 6. SEM image (micrograph) of ZnO nanopowder (**a**) as prepared and (**b**) heat treated at 1200°C. (**c**) EDS of ZnO nanopowder heat treated at 1200°C.

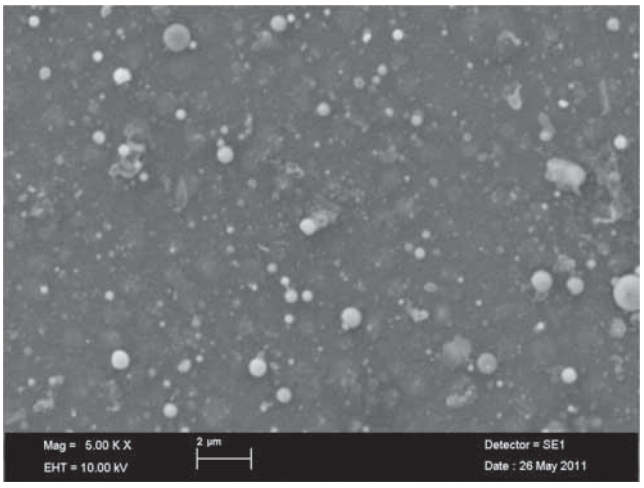

Figure 7. SEM image (micrograph) of ZnO nanopowder heat treated at 1200°C.

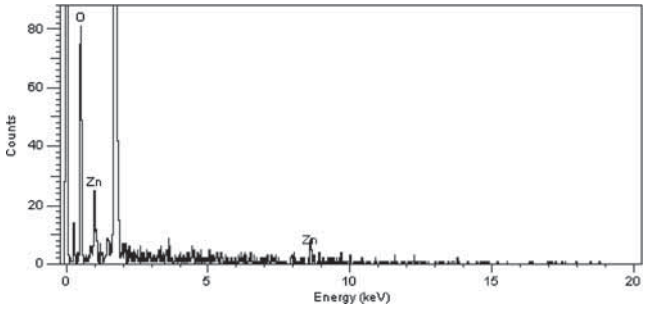

Figure 8. EDS of ZnO nanopowder heat treated at 1200°C.

4. Conclusion

In summary, low temperature aqueous chemical method presented here for the synthesis of ZnO nanopowder is relatively simple, economical and traditionally easy. XRD results revealed purely polycrystalline hexagonal ZnO nanopowder with an average crystallite size 25 nm. PL showed that a strong UV emission at 358 nm corresponds to bandgap (3.47 eV) and particle size (19.4 nm). The green emission observed at 535 nm decreased after heat treatment. Sharpness of UV peak showed that in ZnO nanopowder distribution of ZnO particles size is nearly uniform and narrow. The principle Raman phonon mode observed at 435 cm^{-1} is the characteristic of wurtzite ZnO, while the phonon mode at 1147 cm^{-1} could be associated with second-order phonon Raman scattering processes. The low- and high-frequency Raman peaks appeared at 276 and 970 cm^{-1} for as-prepared sample were no longer found for heat-treated sample and reflected removal of defects in ZnO nanopowders. Zn-O, IR bending and stretching vibrations at wavenumbers 356 and 498 cm^{-1} are the characteristic of Zn–O (υ_{Zn-O}) bonds as established by FT-IR analysis. SEM data confirmed narrow and fine distribution of spherical shape nanocrystallites in the heat-treated sample with no substantial morphological change. Crystallite size determined by two different techniques, XRD and PL, are consistent.

Acknowledgements

We are grateful and wish to thank our parent department, Photonic Division (NILOP) and particularly the nano devices group for the support and providing the required facilities for this research work.

References

1. Look D C 2001 *Mater. Sci. Eng. B* **80** 383
2. Jung S W, An S J and Yi G C 2002 *Appl. Phys. Lett.* **80** 4561
3. Sharma P, Sreenivas K and Rao K V 2003 *J. Appl. Phys.* **93** 3963
4. Sarkar R, Tiwary C S, Kumbhakar P, Basu S and Mitra A K 2008 *Physica E* **40** 3115
5. Zhang D H, Xue Z Y and Wang Q P 2002 *J. Phys. D Appl. Phys.* **35** 2837
6. Hayashi H, Ishizaka A, Haemori M and Koinuma H 2003 *Appl. Phys. Lett.* **82** 1365
7. Ng H T, Chen B, Li J, Han J, Meyyappan M, Wu J, Li S X and Haller E E 2003 *Appl. Phys. Lett.* **82** 2023
8. Chen Y, Bagnall D and Yao T 2000 *Mater. Sci. Eng. B* **75** 190
9. Yao-Chuan Lee, Chen-Ting Lien, Chun-Wan Chen, Sheng-Hsiu Huang, Chih-Chieh Chen, Pei-Chen Kuo, Jin-Yuan Syu, Yuan-Yi Chang, Yi-Mim Huang and Wen-Yinn Lin 2010 *Sustain. Environ. Res.* **20** 397
10. Nasu A and Otsubo Y 2007 *Rheology J. Colloid Interface Sci.* **310** 617
11. Iwasaki T, Satoh M, Masuda T and Fujita T 2000 *J. Mater. Sci.* **35** 4025
12. Sabri M G M, Azmi B Z, Rizwan Zahid, Halimah M K, Hashim M and Zaid M H M 2011 *Int. J. Phys. Sci.* **6** 1388
13. Sudakar C, Kharel P, Lawes G, Suryanarayanan R, Naik R and Naik V M 2007 *J. Phys.: Condens. Matter* **19** 026212
14. Perez-Lopez O W, Farias A C and Marcilio N R 2005 *J. Mat. Chem.* **40** 2089
15. Gümüş C, Ozkendir O M, Kavak H and Ufuktepe Y 2006 *J. Optoelectron. Adv. Mater.* **8** 299
16. Bahadur H, Srivastava A K, Haranath D, Chander H, Basu A, Samanta S B and Kishore R 2007 *J. App. Phys.* **45** 395
17. N Singh, S Mittal, K N Sood, Rashmi and R K Gupta 2010 **7** 297
18. Cho M W, Harada C, Suzuki H, Minegishi T, Yao T, Ko H and Maeda K 2005 *Superlattices Microst.* **38** 349
19. Wang M, Hahn S H, Kim J S, Chung J S, Kim E J and Koo K K 2008 *J. Crystal* **310** 1213
20. Suvaci E and Özer I O 2005 *J. Eur. Ceramic Soc.* **25** 1663
21. Huang A and Caro J 2010 *J. Crystal Growth* **312** 947
22. Choi J H, Tabata H and Kawai T 2001 *J. Crystal Growth* **226** 493
23. Sagar P, Kumar M and Mehra R M 2005 *Mater. Sci.-Poland* **23** 685

24. Venkatachalam R T, Rajendarkumar D, Mangalaraj S K, Narayandass K K and Yi J 2004 *Solid State Electron.* **48** 2219
25. Venkatachalam S and Yoshinori Kanno 2009 *Curr. Appl. Phys.* **9** 1232
26. Cullity B D and Stock S R 2001 *Elements of X-ray diffraction,* 3rd ed (New York: Prentice)
27. Pankove J I 1971 *Optical processes in semiconductors* (New York: Dover)
28. Khan Z R, Arif M and Singh A 2012 *Int. Nano Lett.* **2** 22
29. Dai L, Chen X L, Wang W J, Zhou T and Hu B Q 2003 *J. Phys.: Condens. Matter* **15** 2221
30. Cao H, Zhao Y G, Ong H C, Ho S T, Dai J Y, Wu J Y and Chang R P H 1998 *Appl. Phys. Lett.* **73** 3656
31. Van Dijken A, Meulenkamp E A, Vanmaekelbergh D and Meijerink A 2000 *J. Lumin.* **90** 123
32. Voss T, Bekeny C, Gutowski J, Tena-Zaera R and Bisquert J 2009 *J. Appl. Phys.* **106** 054304
33. Ying Hou, Ming Yang, Guangsheng Pang and Shouhua Feng 2007 *Cryst. Res.* **42** 1068
34. Choi S H, Kim E G, Park J, An K, Lee N, Kim S C and Hyeon T 2005 *J. Phys. Chem. B* **109** 14792
35. Kohan A F, Ceder G and Morgan D 2000 *Phys. Rev. B* **61** 15019
36. Sudakar C, Kharel P, Lawes G, Suryanarayanan R, Naik R and Naik V M 2007 *J. Phys.: Condens. Matter* **19** 026212
37. Loudon R 1964 *Adv. Phys.* **13** 423
38. Tomar M S, Melgarejo R, Dobal P S and Katiyar R S 2001 *J. Mater. Res.* **16** 903
39. Ye J D, Gu S L, Zhu S M, Liu S M, Zheng Y D, Zhang R, Shi Y, Chen Q, Yu H Q and Ye Y D 2006 *Appl. Phys. Lett.* **88** 101905
40. Youn C J, Jeong T S, Han M S and Kim J H 2004 *J. Cryst. Growth* **261** 526
41. Samanta K, Bhattacharya P and Katiyar R S 2006 *Phys. Rev. B* **73** 245213
42. Maensiri S, Laokul P and Pokha S 2006 *J. Magn. Magn. Mater.* **305** 381
43. Coates J 2000 *Interpretation of infrared spectra, a practical approach in encyclopedia of analytical chemistry* R A Meyers (ed) (Chichester: John Wiley & Sons Ltd.) 10815
44. Wang J Z, Peres M, Soares J, Gorochov O, Barradas N P, Alves E, Lewis J E, Fortunato E, Neves A and Monteiro T 2005 *J. Phys. Condens. Matter* **17** 1719
45. Du Y, Zhang M-S, Hong J, Shen Y, Chen Q and Yin Z 2003 *Appl. Phys. A* **76** 171
46. Nakamoto K, *Infrared and Raman spectra of inorganic and coordination compounds parts A and B* (New York: John Wiley & Sons) 1997
47. Andrés-Vergés M and Serna C J 1988 *J. Mater. Sci. Lett.* **7** 970
48. Masoud Salavati-Niasari, Fatemeh Davar and Mehdi Mazaheri 2008 *Mater. Lett.* **62** 1890
49. Ristic M, Music S, Ivanda M and Popovic S 2005 *J. Alloys Compd.* **397** L1